Preprint: *J. IES*, **30**-1, 105-115 (2001)

Integrating Sphere Simulation on Spatial Nonuniformity Errors in Luminous Flux Measurement

Yoshi Ohno[†] and Ronald O. Daubach[††]

[†]National Institute of Standards and Technology
100 Bureau Drive, Stop 8442, Gaithersburg, MD 20899
Phone: (301) 975-2321, Fax: (301) 840-8551
Email: ohno@nist.gov

[††]OSRAM SYLVANIA
71 Cherry Hill Drive, Beverly, MA 01915
Phone: (978) 750-1593, Fax: (978) 750-1794
Email: ronald.daubach@sylvania.com

Abstract

To obtain general knowledge on the spatial nonuniformity errors of an integrating sphere photometer associated with the spatial intensity distributions of test lamps, a series of computer simulations have been conducted for various designs of an integrating sphere measuring different types of lamps. An integrating sphere simulation program, previously developed for the realization of the luminous flux unit at NIST, has been utilized for this analysis. The program simulates interreflections in an integrating sphere and calculates the final luminance distributions on the sphere wall as well as the detector output. Using this program, simulations have been conducted on a 2 m integrating sphere having a 30 cm circular baffle, with varied sphere wall reflectance (ρ = 80 % to 98 %) and baffle reflectances, the size and location of the baffle, and the angular response of the detector. Measurement errors (with respect to an isotropic point source) were calculated for actual intensity distribution data of eight different types of incandescent and discharge lamps. The results show that, with a well-designed integrating sphere photometer with no contamination of coating, measurement uncertainties (k=2) on the order of 1 % (ρ = 80 %) to 0.1 % (ρ = 98 %) can be expected for typical general service lamps with no reflectors, measured against a calibration source of uniform intensity distribution. Larger errors are shown with integrating sphere photometers not properly designed.

Keywords: Calibration, Goniophotometry, Integrating sphere, Lumen, Luminous flux, Photometer, Photometry, Simulation, Standards, Total luminous flux, Uncertainty

Introduction

Integrating sphere photometers are commonly used to measure the total luminous flux of light sources. The substitution method is utilized, in which a test lamp is measured in comparison to a standard lamp. Due to the spatial nonuniformities of integrating spheres – mainly due to existence of a baffle and nonuniform coating, errors can occur when the angular intensity distribution of the test lamp is different from that of the standard lamp. Consequently, test lamps should only be measured against standard lamps of the same or similar type, as recommended in standard pracitices[1, 2]. However, due to limited types of standard lamps available, test lamps are very often measured against different types of standard lamps. In such cases, the errors can be serious but the magnitude of errors has not been well known, and has been one of the largest uncertainty components of luminous flux measurements in industry.

General theories of integrating spheres are well established[3]. The theoretical analysis of the effects of a baffle in an integrating sphere is complex, but numerical solutions became available[4-6]. These analyses have been useful, but are limited to axially symmetric sphere geometries, thus to rather simple applications. In 1994, as a part of the research on the realization of the lumen at National Institute of Standards Technology (NIST), a computer simulation program based on the flux tracing technique was developed, which has allowed analyses on axially asymmetric geometries with two baffles in an integrating sphere[7]. The simulation with this program agreed well with the experimental results to test the effects of baffles[8].

Recently, experimental analyses were made on the spatial nonuniformity errors of the integrating sphere used at NIST – the 2 m sphere[9,10] and the new 2.5 m sphere[11] – for measurements of incandescent standard lamps. While some knowledge was obtained on the magnitude of errors, the results were not applicable to other integrating spheres in general and for more varieties of lamp types.

To obtain more general knowledge on the errors of various integrating sphere photometers for varieties of lamps produced in the lighting industry, a series of simulations have been conducted using the NIST simulation program. Simulations were made on an integrating sphere photometer with varied parameters including reflectance of the sphere wall and baffle surfaces, location and size of the baffle, and angular responsivity of the detector. Measurement errors (with respect to an isotropic point source) were calculated for actual intensity distribution data of many different types of incandescent and discharge lamps measured at the Osram Sylvania laboratory. From the results, the magnitude of errors and the effects of each parameter of the sphere photometer are discussed.

Integrating sphere simulation program

The program is based on the flux tracing technique. A sphere surface is divided into 2592 elements (5° step on θ and ϕ), and the luminous flux falling on each element reflected from all other elements and baffle surfaces is calculated for each interreflection. The calculation starts with the initial illuminance distribution produced by an internal light source having a given intensity distribution, and the interreflection is repeated until the initial flux is mostly absorbed (98 % was used this time) by the sphere surfaces. Comparisons of results with a setting of 99.9 % absorption indicated errors in the sphere response factors (see later section) within 0.1 %. The program finally calculates the luminance distributions on the sphere wall and on baffle surfaces as well as the detector output taking into account the angular responsivity of the detector. The simulation assumes Lambertian reflectance factor for all surfaces. Real sphere coating surfaces are nearly Lambertian, and the effect of the differences from this assumption is considered negligible. A simulation on a real integrating sphere showed sufficient agreement with the measured results (see section *Analysis of SRDF*). Reference 7 should be referred to for further details on the algorithm of the simulation.

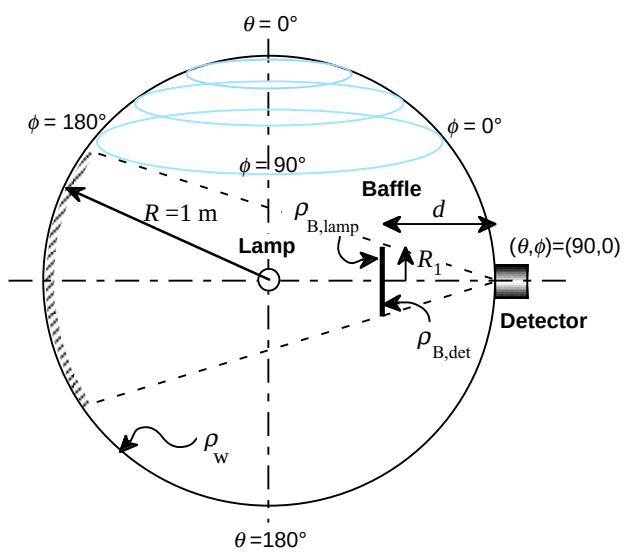

Figure 1 – Parameters for the integrating sphere model

The integrating sphere model used in this simulation is shown in **Figure 1**. The layout of the detector and the polar coordinate system represent a typical layout of an integrating sphere photometer and the format of goniophotometric data of lamps used in industry. The radius R of the sphere is fixed to 1 m (2 m diameter sphere). The default condition is a 30 cm baffle located at half way between the lamp and the detector (d = 0.5 m, R_1 = 0.15 m, ρ_w = 80%). These parameters are varied to simulate different sphere designs. The angular responsivity of the detector is a perfect cosine response as default, and also a modified response for varied field of view can be added. **Figure 2** shows the modified detector response curve used this time, which represents a photometer head with a flat diffuser that is not perfectly diffusive. A very narrow-field of view of a detector is often found in spectrophotometric applications, but it would cause serious errors if used for luminous flux measurement of lamps. In this simulation program, the luminance on the detector-side of the baffle is also calculated to represent a narrow field of view of the detector.

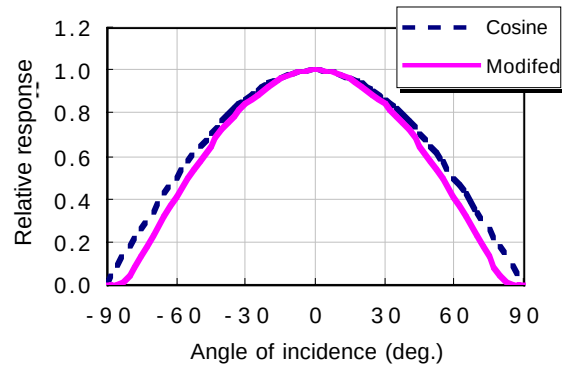

Figure 2 – Two curves of the detector angular responsivity used in the simulation

Test lamps for simulation

Initially, 24 different types of commonly produced incandescent and discharge lamps were selected for use in the simulation. The lamps are products of Osram Sylvania Inc.(OSI)[†] and the luminous intensity distributions (LIDs) of these lamps were measured using the goniophotometer at OSI laboratory in Beverly, Massachusetts. The data were taken at intervals of 0.1° for longitudinal angle θ and 10° for azimuth angle ϕ, and then converted to 5° intervals for both θ and ϕ to fit the data format of the simulation program. Since the simulation was very time consuming, the LID curves of these lamps were examined for similarity, and seven lamps representing different types as listed in **Table 1** were selected for use in the simulation. A computer model of a linear fluorescent lamp in horizontal operation was also added as a test lamp. Actual intensity distributions of the linear fluorescent lamps are close to this model. The LID curves of these eight lamps are shown in **Figure 3**.

Table 1 – Lamps used for analysis by simulation

No.	Type	Abbreviation	Model
1	Incandescent	INC	150W/130V A-21 Excel-Line Inside Frost
6	Reflector-type	PAR	75W/120V PAR-30 Capsylite Flood
12	Compact Fluorescent	CFL-1	11W Double Twin Tube CF NAED 29107
16	Compact Fluorescent	CFL-2	7W Twin Tube CF NAED 20327
18	Metal Halide	MH	100W Clear Pro-Tech Metalarc
20	High-pressure Sodium	HPS	100W Clear High Pressure Sodium Lamp
24	Circular Fluorescent	CIRC	FC8T9/CB/RS Circline Fluorescent Lamp
	Linear Fluorescent	LIN-FL	Computer model of a horizontal line source

[†] Specific firms and trade names are identified in this paper to specify the experimental procedure adequately. Such identification does not imply recommendation or endorsement by the National Institute of Standards and Technology, nor does it imply that the materials or equipment identified are necessarily the best available for the purpose.

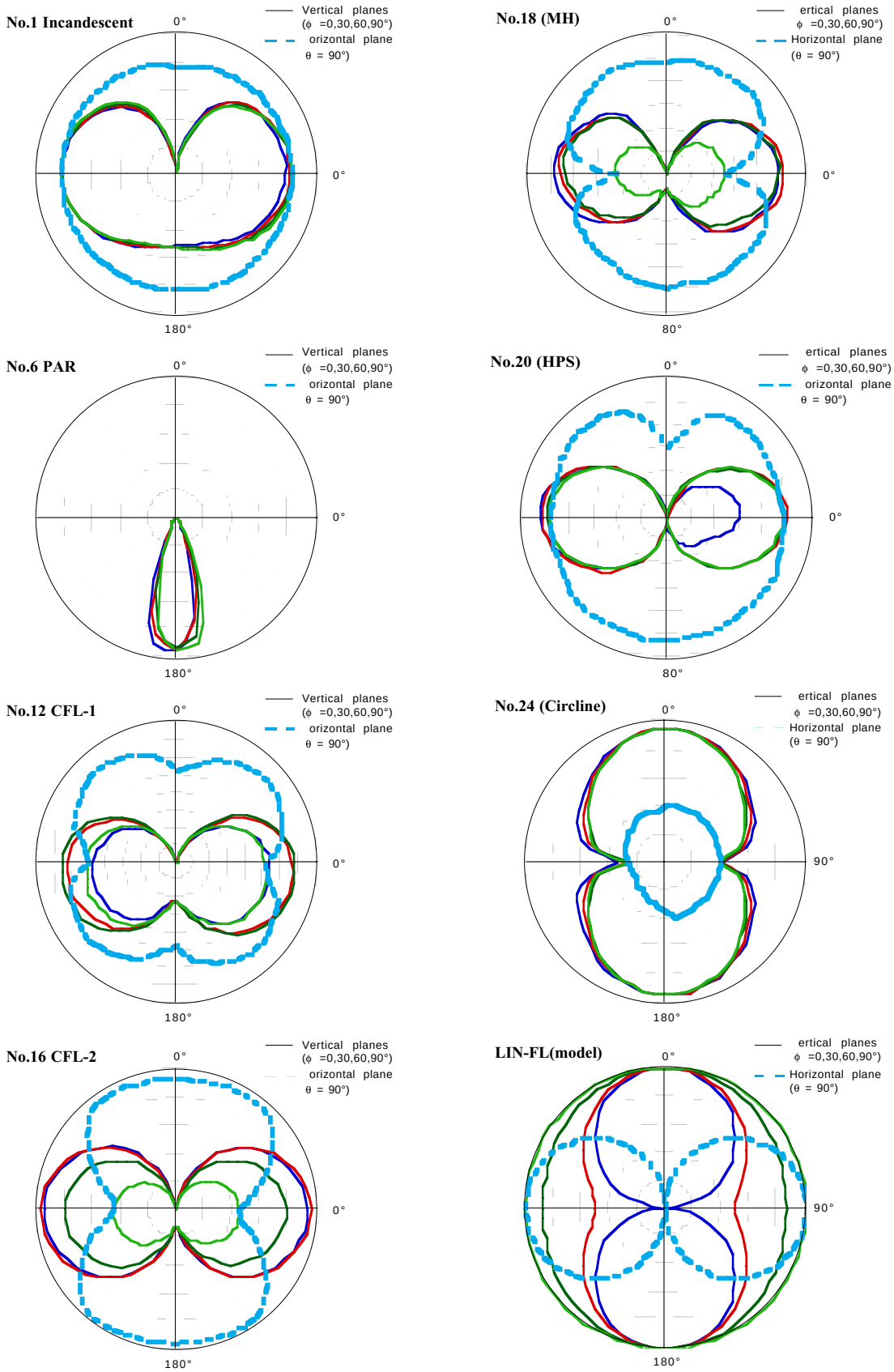

Figure 3 – Luminous intensity distributions of the lamps used in the simulation

Results of simulation

The simulation was conducted under varied sphere parameters as shown in **Table 2**. The parameters in the table are defined in **Figure 1**. The parameters changed from the default condition (Condition 1) are highlighted in the table. For each condition, the output of the detector is calculated for both cosine response and for the modified response (**Figure 2**) and for a very narrow field of view (luminance of the baffle surface on the detector side). The reflectance value of 80 % is chosen as the default since this value is generally recommended by CIE[1] for integrating sphere photometers. The simulation is conducted up to 98 % reflectance since actual integrating spheres used throughout the world use various reflectances in this range. The default value of the baffle (30 cm diameter at 1/2 point between the lamp and the detector) is chosen to be large enough to shield most of large-size discharge lamps (except tubular lamps) used for general lighting.

Table 2 – Conditions of the integrating sphere for simulation

Condition	parameter changed	ρ_w	$\rho_{B,lamp}$	$\rho_{B,det}$	R_1	d
1	Default	80	80	80	0.15	0.5
2	Baffle size	80	80	80	0.10	0.5
3	Baffle size	80	80	80	0.21	0.5
4	Baffle location	80	80	80	0.15	0.25
5	Baffle size/location	80	80	80	0.075	0.25
6	Baffle reflectance	80	98	98	0.15	0.5
7	Baffle reflectance	80	80	0	0.15	0.5
8	Wall reflectance	90	90	90	0.15	0.5
9	Wall reflectance	98	98	98	0.15	0.5

Analysis of SRDF

The simulation was first conducted to obtain the Spatial Response Distribution Function (SRDF) of the integrating sphere for each condition. The SRDF is the relative responsivity of the sphere (detector signal per input flux) as a function of the location (θ,ϕ) of the sphere wall including baffle surfaces, and is used to calculate measurement errors associated with LIDs of lamps[9, 10]. The SRDF can be measured by scanning a narrow beam in a real integrating sphere. In the simulation, it is obtained by a program loop repeating the simulation with the initial flux incident only on one surface element, the location of which is scanned over the entire sphere surfaces. Since this is a very time-consuming operation, the SRDF values were obtained for only one hemispherical plane from (90°,0°) to (90°, 180°) at 5° intervals (36 points) and interpolated to all the sphere elements (2592 points) utilizing axial symmetry. The position (90°,0°) is on the center of the baffle.

Once the relative SRDF, $K(\theta,\phi)$ is obtained, it is normalized to the sphere response for an isotropic point source, as given by

$$K^*(\theta,\phi) = \frac{4\,\pi\,K(\theta,\phi)}{\int_{\phi=0}^{2\pi}\int_{\theta=0}^{\pi} K(\theta,\phi)\,\sin\theta\,\mathrm{d}\theta\,\mathrm{d}\phi} \tag{1}$$

The values of $K^*(\theta,\phi)$, therefore, directly indicate the responsivity of the sphere at that point (θ,ϕ) relative to the average response over the entire sphere.

The normalized SRDF map obtained by the simulation for the default condition is shown in **Figure 4** as an example. The polar coordinate (θ,ϕ) corresponds to the layout shown in **Figure 1**. The center of the area (90°,0°) is the detector, and the hollow at the edges is the region where the detector's view is intercepted by the baffle (shadowed region in **Figure 1**). The hollow and the hump on the SRDF map are the causes of measurement errors associated with LIDs. The deep hollow on the center is the region where light from the sphere center hits the baffle surface. The hump around the center is the region where light from the sphere center hits the sphere wall near the detector. This hump is caused by the interreflections between the sphere

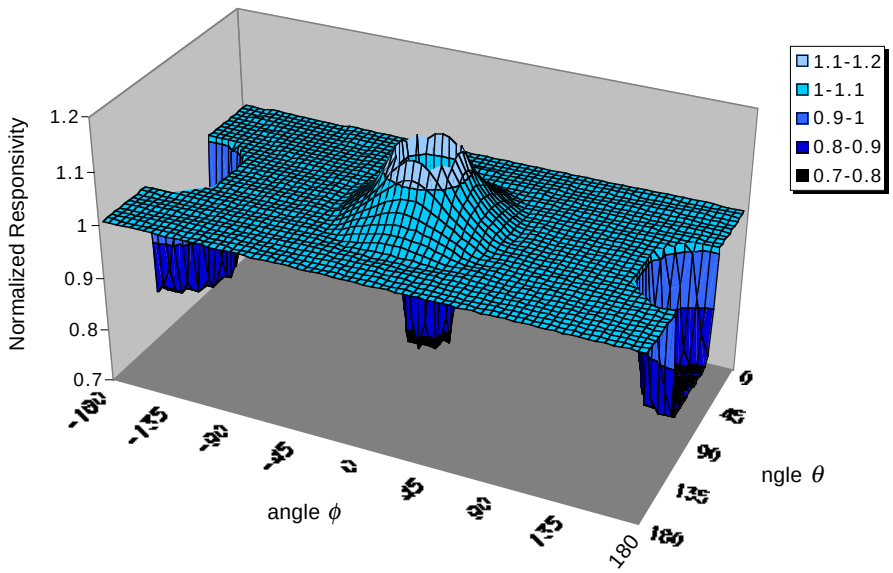

Figure 4 – The SRDF of the integrating sphere in the default condition.

wall (around the detector) and the baffle surface, which results in higher luminances on these surfaces, and thus higher detector response. The sphere response at the hollow regions (on the baffle surface and the shadowed region) is about 80 % of the other flat region in this condition, which approximately corresponds to the reflectance of the sphere wall. This is explained by the fact that the first reflection from these regions does not reach the detector, causing a relative detector signal loss of 1-ρ.

For verification of the simulation program, a measurement was made on the NIST 2.5 m integrating sphere (~98 % reflectance coating) using a scanning beam source[11], and was compared with the simulation result as shown in **Figure 5**. Although the measurement curve is much affected by the nonuniformity of the coating and other factors, the basic forms of the two curves agree well and it is shown that the simulation predicts the effects of the baffle (hollows and humps) accurately.

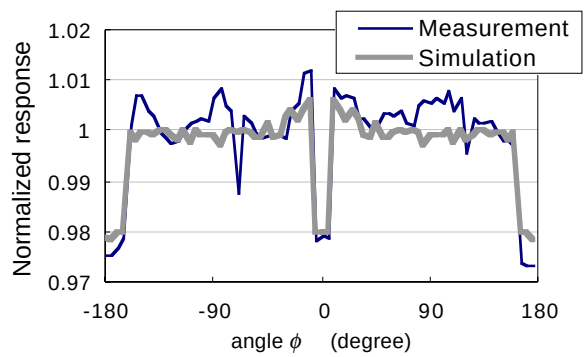

Figure 5 – SRDF curves on the equatorial plane of the NIST 2.5 m sphere obtained by the simulation and by measurement. The two downward spikes on the measurement curve are the seams of the sphere.

Calculation of the sphere response factor

The errors associated with various LIDs of lamps are evaluated by the sphere response factor, f_s, which is defined as the ratio of the sphere response (detector signal) for a light source of a given LID to that for an isotropic point source having the same luminous flux[10]. The f_s is calculated using the normalized SRDF, $K^*(\theta,\phi)$, by

$$f_s = \frac{\int_{\phi=0}^{2\pi} \int_{\theta=0}^{\pi} I_{\mathrm{rel}}(\theta,\phi)\, K^*(\theta,\phi) \sin\theta \,\mathrm{d}\theta \,\mathrm{d}\phi}{\int_{\phi=0}^{2\pi} \int_{\theta=0}^{\pi} I_{\mathrm{rel}}(\theta,\phi) \sin\theta \,\mathrm{d}\theta \,\mathrm{d}\phi} \qquad (2)$$

where $I_{rel}(\theta,\phi)$ is the relative LID of the test lamp. The f_s is unity for an isotropic source, and thus the measurement error for each test lamp is given by $f_s - 1$ when the sphere is calibrated with an isotropic source.

The LIDs of the real lamps are not axially symmetric, and thus, the f_s value for a given LID for a given sphere condition can vary significantly depending on the horizontal rotation angle of the lamp when mounted in the sphere. Therefore, for each lamp at each sphere condition, the f_s value was calculated for each horizontal rotation of the lamp at 5° intervals over one rotation (0 to 355°), and the range of the f_s values for the rotation was evaluated. Therefore, f_s was calculated for 72 (lamp rotation) x 8 (lamps) x 9 (sphere conditions) = 5184 times. As an example, the plots of f_s for lamp #16 (CFL-2) in the default sphere condition are shown in **Figure 6**.

Then, the ranges of the f_s value (due to rotation) for all the eight lamps in each sphere condition are plotted as in **Figure 7**. Each bar in the graph indicates the range of the f_s value for lamp rotation. The change (length of the bar) is small for lamps having nearly axially symmetric LIDs such as INC and PAR. The change is large for axially nonuniform lamps such as CFL-2 and LIN-FL. Similar graphs were made for all the sphere conditions, and it was observed that the patterns of the plots were rather similar, with different scales under varied conditions. Thus, to present many results in a limited space, the eight lamps have been grouped into three: Group 1 (INC, CFL-1, CFL-2, MH, HPS), Group 2 (CIRC, LIN-FL), and Group 3 (PAR), and the ranges of f_s were recalculated for each group. The lamps in Group 1 have rather horizontally enhanced LIDs exhibiting slightly lower response, whereas, the lamps in Group 2 have more vertically enhanced LIDs exhibiting slightly higher response. Group 3 (PAR) is a narrow beam illuminating downwards with very little light incident on the baffle or the shadowed region, thus exhibiting much higher response than the others. Further analyses are made and presented using the data reduced in this manner.

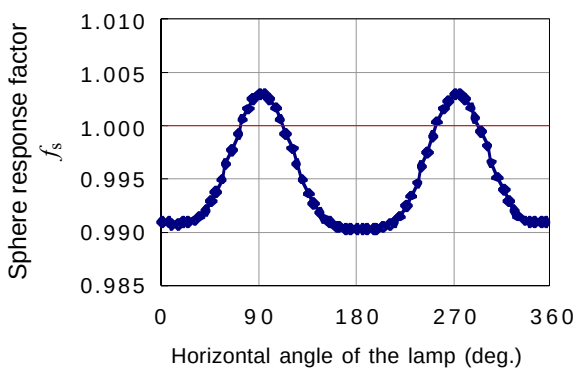

Figure 6 – Change of the sphere response factor f_s of lamp#16 (CFL-2) with horizontal rotation of the lamp for the default sphere condition.

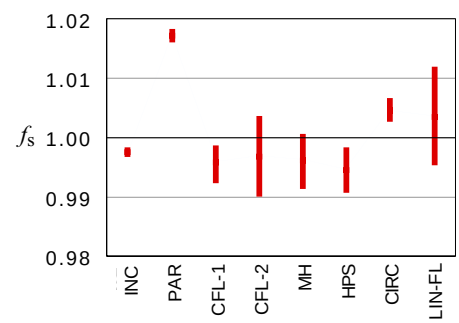

Figure 7 – The range of the sphere response factor when each lamp is horizontally rotated for 360° in the sphere – default condition.

Effect of the baffle size

Figure 8 shows the effect of the varied size of the baffle – 20 cm, 30 cm, and 42 cm diameters. **Figure 8 (a)** shows the SRDF curves of the sphere at θ=90° (equatorial plane), and shows that the center hump and the hollow around θ=±180° become wider with increased size of the baffle. **Figure 8 (b)** shows the plots of the f_s values for each group of lamps for each baffle size. By comparing the results for three baffle sizes, it can be seen that the errors increase with increased size of the baffle, approximately proportional to the diameter of the baffle. The effect is less proportional to the area of the baffle because, as seen in the SRDF plots, the central hump also grows and works to compensate a part of the negative error by the hollows (for symmetrically distributed lamps). The results of this simulation clearly indicate that the size of the baffle is a critical factor for the errors and that it is important to keep the size of the baffle smallest possible.

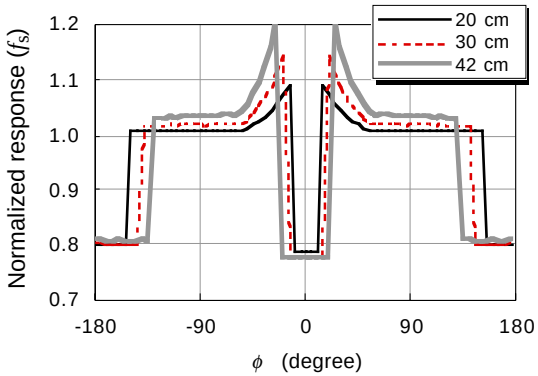

(a) SRDF plot at θ=90°

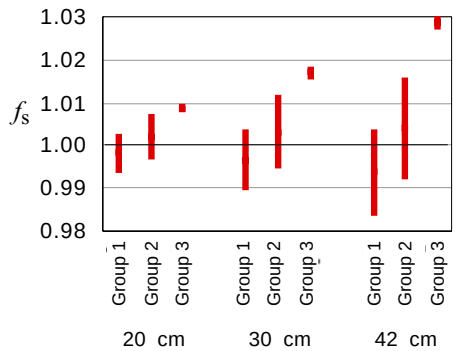

(b) Range of the sphere response factor

Figure 8 – The effect of varied size of the baffle (Conditions 2, 1, 3). The values (20 cm, 30 cm, 42 cm) indicate the diameter of the baffle.

Effect of the reflectance of baffle surfaces

Figure 9 shows the effect of varied reflectance of the baffle surfaces, comparing 1) the default condition when both sides of the baffle are 80 % reflectance, 2) when both sides of the baffle are 98 %, 3) when one side of the baffle facing the detector is 0 % reflectance (black). The plots of the f_s values in **Figure 9 (b)** show notable reduction in errors with the 98/98% condition, and increase in errors with the 80/0% condition. The SRDF curve for 98%/98% condition in **Figure 9 (a)** shows that the center hollow is lifted up to ~0.95 (other cases, ~0.8), which is an effect of higher reflectance on the baffle surface facing the lamp and is effective in reducing the errors. The higher reflectance on the detector side produces higher central hump of the SRDF, which actually helps compensate for the negative errors caused by the hollows. A black surface on the detector side of the baffle (the 80/0 condition) would cause a wide center hollow rather than a hump, which leads to increased errors.

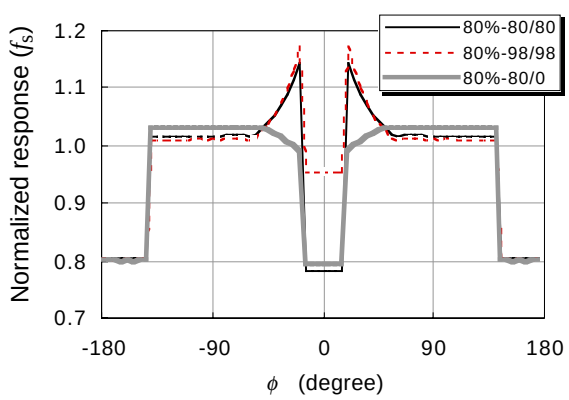

a) SRDF plot at θ=90°

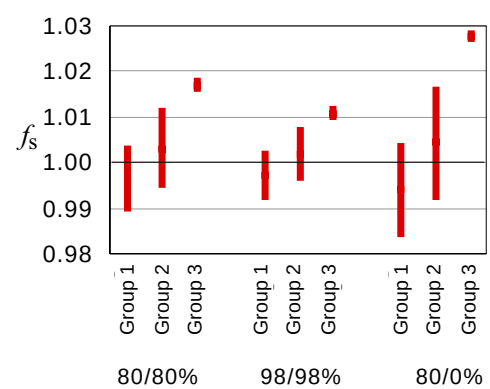

(b) Range of the sphere response factor

Figure 9 – The effect of varied reflectance of the baffle surfaces (Conditions 1, 6, 7). "80%-80/0", e.g., means that the reflectance of the sphere wall is 80% and the reflectance of the baffle is 80 % on the lamp side and 0 % (black) on the detector side.

Effect of the reflectance of the sphere wall

Figure 10 shows the effect of varied reflectance of the sphere wall, comparing 80 %, 90 %, and 98 %. Baffle reflectances are set to be the same as the sphere wall reflectance for simplicity. The SRDF curves in **Figure 10 (a)** shows a dramatic improvement of uniformity with 98 % reflectance, and the plots of f_s values in **Figure 10 (b)** also show remarkable improvements with higher reflectances. The measurement errors $(f_s - 1)$ for all types of lamps are within 2 % for 80 %, 1 % for 90 % and 0.2 % for 98 % reflectance, which proves that the errors associated with LID of lamps are proportional to $1\text{-}\rho_w$. The range of errors will be nearly half if Group 3 (reflector lamp) is excluded.

It should be noted, however, that errors due to other causes (such as self-absorption of the test lamp, spectral variation of coating reflectance, drift of the sphere responsivity due to contamination, mechanical repeatability of the sphere closing, etc.) become more sensitive with higher reflectances and can be much higher than the errors discussed in this paper. Higher reflectance of the sphere coating is preferred if other sources of errors are well controlled or corrected.

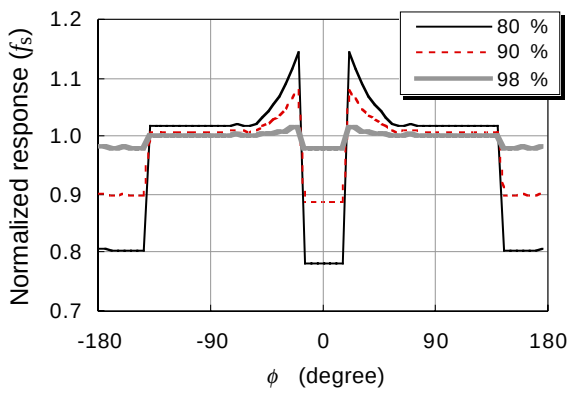

(a) SRDF plot at θ=90°

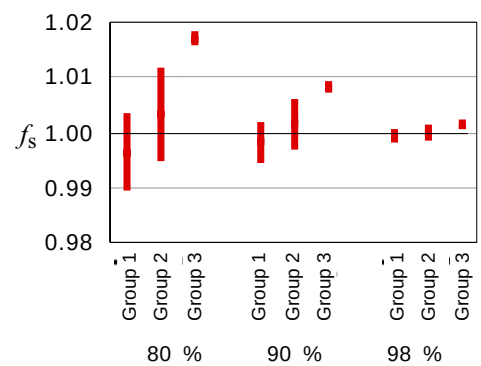

(b) Range of the sphere response factor

Figure 10 – The effect of varied reflectance of the sphere wall. (Conditions 1, 8, and 9)

Effect of the detector angular response

The simulation program calculated all the results for 1) cosine response, 2) modified response shown in **Figure 2**, and 3) very narrow field of view (measuring the luminance of the baffle). **Figure 11** shows one of the results (for the default condition). First, for comparison of the cosine response and the modified response, the SRDF curves in **Figure 11 (a)** show that the central hump is flattened out with the modified detector (due to the reduced responsivity at larger angles). This makes no compensation to the negative errors by the hollows, leading to increased errors (about 1.5 times) as shown in the f_s plots "Modified" in **Figure 11 (b)**. In some other cases, the increase of errors by the modified detector is even larger than shown here. Generally, not much attention is paid to cosine correction of the detectors for integrating spheres, and in some cases one can find spheres using detectors much poorer than the simulated model used this time, where much larger errors are expected. These results show that cosine correction for a sphere photometer is actually very important.

The extreme case is a very narrow field of view of the detector. There has been some misconception afloat that, by viewing only the backside of the baffle (its luminance), the detector never sees the first reflection and thus has better performance. This is completely wrong, which is proved by this simulation. The curve labeled "Baff. Lum" in **Figure 11 (a)** shows the SRDF curve for this condition that produced surprisingly high hump around the baffle. In **Figure 11 (b)**, the range of f_s for this condition is shown separately on the right hand side with different scale. The errors are several times larger than the cosine response, and even the direction of the errors is reversed (because the central hump dominates the

nonuniformity in SRDF). This tragic result can be explained by the fact that the luminance on the detector-side of the baffle is produced by reflections from a large part of the sphere wall around the detector, which acts as a large-area detector that are not shielded from direct illumination by the lamp.

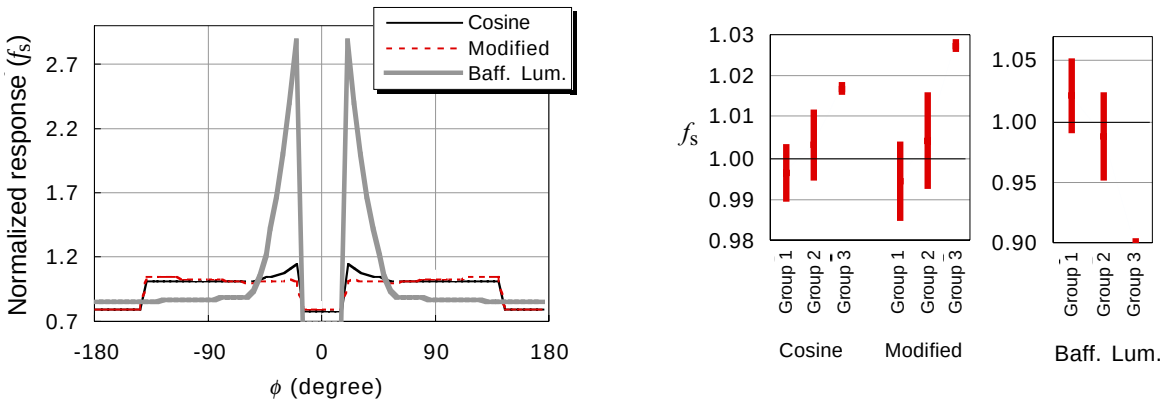

(a) SRDF plot at θ=90°

(b) Range of the sphere response factor

Figure 11 – The effect of the angular responsivity of the detector.

Location of the baffle

Simulation was also conducted changing the location of the baffle. **Figure 12** shows the results for 1) 30 cm baffle at 0.5 *R* (default), 2) 15 cm baffle at 0.25 *R* (the shielding angle from the detector is kept the same), and 3) 30 cm baffle at 0.25 *R* (baffle simply moved closer to the detector). The SRDF curves in **Figure 12 (a)** show that, when the baffle is closer to the detector (0.25 *R*), the central hump becomes very high due to enhanced interreflection effects. While this helps to compensate for the negative errors by the hollow (as seen in **Figure 12 (b)** showing reduced errors for 15cm/0.25*R* condition), the very high center hump is rather dangerous for measurement of lamps with asymmetric LIDs (not included in the analysis this time). In addition, the f_s values for the 15cm/0.25*R* condition with the modified detector did not show improvements. The observation of the SRDF curves implies that the baffle should not be placed too close to

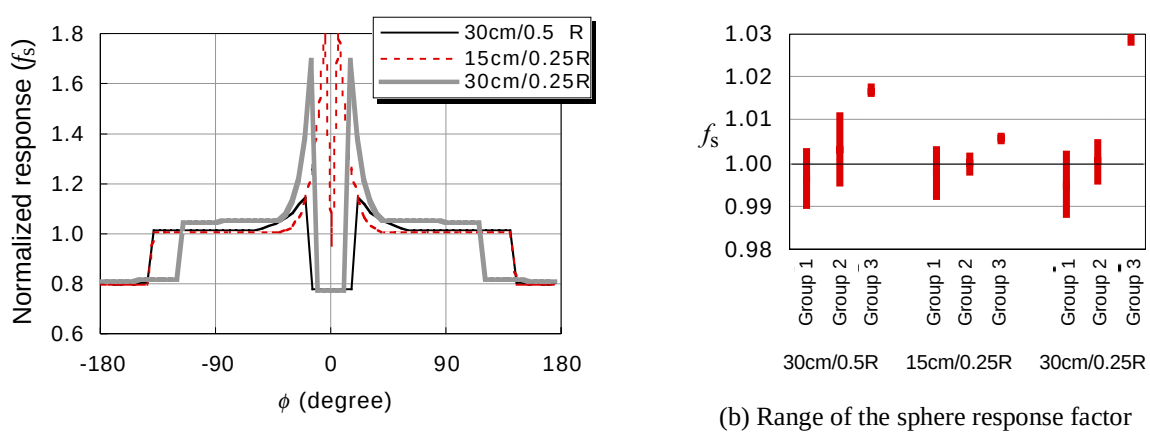

(a) SRDF plot at θ=90°

(b) Range of the sphere response factor

Figure 12 – The effect of varied location (and size) of the baffle (Conditions 1, 4, 5). 30cm/0.5R, e.g., indicates a baffle of 30 cm diameter located at 0.5 sphere radius from the detector.

the detector even with reduced size. A separate calculation shows that the total area of the hollows (by the baffle and by the shadow of the baffle) is minimized at the baffle location around 1/3 R to 1/2 R from the detector, which is verified to be appropriate.

Conclusions

There have been many findings from this simulation study. The magnitude of the errors in sphere photometry associated with LIDs of lamps has been indicated for various types of real lamps and for various sphere designs. From the results, with a well-designed integrating sphere photometer with no contamination of coating, measurement uncertainties (k=2) on the order of 1 % (ρ= 80 %) to 0.1 % (ρ = 98 %) can be expected for typical general service lamps with no reflectors and 2 % (ρ= 80 %) to 0.2 % (ρ= 98 %) for reflector-type lamps in base-up operation, measured against a calibration source of uniform LID. These results will be useful for uncertainty budget analyses of general sphere photometry.

The effects of various design parameters of an integrating sphere have been quantified in relation to the measurement errors in luminous flux, which will be useful in designing or improving integrating spheres for reduced uncertainties. For example, the results indicated the degree of improvements by higher reflectance of the sphere wall and baffle surfaces, as well as by good cosine correction of the detector. It has also been shown that use of narrow-field of view of the detector would be disastrous for integrating sphere photometers.

The LIDs and associated measurement errors for many different types of lamps examined this time are not as diverse as was expected. For example, all the lamps in Group 2 can be calibrated against an incandescent standard lamp within acceptable uncertainty (in terms of spatial distribution only). Reflector-type lamps of various beam angles can probably be measured against one type of reflector lamp within acceptable uncertainty (if the bottom of the sphere is clean). It is also verified that a linear (tubular) lamp needs to be calibrated against a linear lamp mounted in the same direction. Such a calibration may be difficult for fluorescent lamps, as they are generally not stable enough. Instead, a correction factor can be obtained from the SRDF and applied to the results, or such an effect should be included in the uncertainty budget.

Finally, the effect of contamination of the sphere wall (nonuniform reflectances) has not been analyzed in this study. The contamination normally causes unbalanced reflectances for upper half and lower half of the sphere, which causes errors for lamps having vertically unbalanced flux distributions, and local nonuniformities of contamination affects especially measurement of reflector-type lamps. Further study is needed in this respect.

References

1. CIE. 1989. *Publication No. 84 Measurement of luminous flux*.
2. IES. 1993. Lighting Handbook 8th Edition – Reference and Application
3. for example: J. Jacquez and H. Kuppenheim. 1955. Theory of the integrating sphere, *J. Opt. Soc. Am*. **45**: 460-470.
4. F. Rotter. 1971. View into the integrating sphere through the observation window, *Appl. Opt*. **10**: 2629-2638.
5. R. Brown. 1973. A numerical solution of the integrating sphere through the observation window, *J. Res. Natl. Bur. Stand*. Sect. A **77**: 343-351.
6. A.C.M. de Visser and M. van der Woude. 1980. Minimization of the screen effect in the integrating sphere by variation of reflectance factor, *Light. Res. Technol*. **12**: 42-49.
7. Y. Ohno. 1994. Integrating Sphere Simulation - Application to Total Flux Scale Realization, *Appl. Opt*. **33**(13): 2637-2647.
8. Y. Ohno. 1995. New Method for Realizing a Total Luminous Flux Scale using an Integrating Sphere with an External Source, *J. Illum. Eng. Soc*. **24**(1): 106-115.
9. Y. Ohno. 1996. Realization of NIST 1995 Luminous Flux Scale using Integrating Sphere Method, *J. Illum. Eng. Soc*. **25**-1: 13-22.
10. Y. Ohno, M. Lindemann, and G. Sauter. 1997. Analysis of integrating sphere errors for lamps having different angular intensity distributions, *J. Illum. Eng. Soc*. **26**(2): 107-114.
11. Y. Ohno and Y. Zong. 1999. Detector-Based Integrating Sphere Photometry, *Proc., 24th Session of the CIE*, **1**-1: 155-160.

Discussion

The authors provide a very useful simulation of the magnitude of the errors in spherical photometry caused by the presence of the (necessary) baffle. While it was generally known that the parameters studied were the source of errors, the magnitude of the errors was not previously known as comprehensively as presented. I expect that application of the knowledge gained will greatly help the industry achieve more uniform results in photometric measurements of all products.

I was most surprised by the strong effects of the detector angular response. This points out a source of error that we, at least, had not taken into account as should have been done. With the increasing use of spectral diode array systems using fiber optic cables connected to the sphere for obtaining spectral data it seems to me to be very important to consider the detector response of such a sensor. Without a diffusing filter, fiber optic cables tend to have an angular response about that of the baffle used in the simulation. Thus the use of a diffusing filter with good cosine correction in front of the fiber optic input is essential. Would the authors discuss how best to choose and install such a diffusing element.

The length of the linear fluorescent lamp used in the test is not stated. However, it is assumed that the length is less than 60 cm (2 ft), otherwise it could not be rotated behind a circular baffle as depicted in Figure 7. Could the authors state the fluorescent lamp length used.

Finally, it is stated in the conclusion that It is verified that a linear (tubular) lamp needs to be calibrated against a linear lamp mounted in the same direction. This idea is good in principle but has not been practiced in the industry. Since the variation in lumen output of a given linear fluorescent lamp, at rated current, is about the same size as the f_s error found in the simulation, how do the authors propose to accomplish the use of linear calibration lamps?

Rolf S. Bergman
GE Lighting

Dr. Ohno and Dr. Daubach have prepared a very complete method for evaluating the impact of sphere design and detector capability on the measurement uncertainty for several different lamp types. Using their method, they have been able to show the advantages of new coatings and the importance of the detector used in the sphere. I have three questions for the authors:

1) Spectral corrections were mentioned but not described in the paper. Has there been any consideration made to the addition of the spectral mismatch to the simulation and was there any spectral correction when the lamps were measured on the goniophotometer?

2) The lamps were categorized into groups based on the Intensity Distribution. Was more than one PAR distribution used? Could the authors speculate on the impact of the PAR distribution to the measurement uncertainty?

3) No field verification of the uncertainty calculation was performed. Obviously, it is difficult to modify the design of a sphere in order to verify the simulation but was there an evaluation of the measurement uncertainty for a group of lamps as compared to the model conducted with the basic sphere design?

Again, I would like to thank the authors for their continued work in this area.

Ron B. Gibbons
Philips Lighting

The information reported should be of great interests to lamp manufacturers and the lighting community, as well as integrating sphere photometer manufacturers.

You have provided a comprehensive description of the sources errors and corrections for the measurement of lamps of various intensity distributions placed in the center of an integrating sphere photometer. Presented is a useful tool for further explaining the design and application complexities of the conceptually simple integrating sphere. Many applications require the test source reside outside the integrating sphere photometer. Optical radiation is introduced into the sphere from a port located on the equator. The source types range from reflector lamps to lasers and laser diodes. A laser creates a virtual source opposite the entrance port. Pending integrating sphere design the luminance distribution at the detector port can be very sensitive to the source intensity distribution or alignment. For this application the spatial response distribution function can be measured by placing a narrow beam source at the entrance port and scanning hemispherical, but many end users may find this a daunting tasks. Have you, or do you have any plans to utilize the simulation program for measurement of light sources positioned at the sphere wall on the equator?

Greg McKee
Labsphere Inc.

Author s response

To Dr. R. Bergman

The angular response of the detector for sphere photometers is indeed a very important aspect that is often neglected. Fiber optics of spectroradiometers used for a sphere photometer should also be well cosine-corrected. At NIST and OS, we use surface-ground opal glass for cosine correction of the photometer head as well as for the fiber input optics of a spectroradiometer.

Regarding the length of the linear fluorescent lamp, the size of lamp is ignored in our simulation. The simulation assumes that the test lamp is within the size shielded by the baffle as you pointed out. If a four-foot linear fluorescent lamp is rotated in a 2 m sphere, e.g., the effect would be much larger due to a much larger (rectangular) baffle needed to shield the lamp at any rotation angle.

About the calibration of the sphere for linear fluorescent lamp, the sentence in the conclusion stated it only in terms of spatial distribution. We agree that it would be difficult to calibrate the sphere with fluorescent lamps in practice as they are generally not stable enough. We suggest that, if the sphere is calibrated with an incandescent standard lamp, a correction factor can be obtained from the SRDF and applied to the results, or such an effect should be included in the uncertainty budget. This has been clarified with additional sentences in the conclusion.

To R. Gibbons

1) The nonunifomity of spectral mismatch correction factors over the sphere surfaces is considered negligible, and thus we believe spectral mismatch can be treated separately from the spatial nonuniformity errors discussed in this paper. Thus we do not plan to implement it in this simulation. However, in the coming NIST project for realization of total spectral radiant flux, we plan to do the sphere simulation spectrally. No spectral mismatch correction was applied to the goniophotometric data in the paper because the absolute accuracy of the data was not relevant in this work.

2) We have simulation results for eight different types of PAR lamps ranging from 10¡ to 50¡ beam angles. The results of the simulation (average values of f_s) were similar for all these lamps, and therefore, the result of only one PAR lamp was used in the paper. As shown in the results, if the sphere is calibrated with an ordinary incandescent standard lamp, the error for PAR lamps will be the largest among the lamp types. We suggest the sphere be calibrated with a PAR standard lamp or a correction factor be obtained and applied. The contamination of the sphere is another major uncertainty component for PAR lamps.

3) One measurement comparison was made for the NIST sphere as shown in Figure 5. It is difficult to verify this in various other sphere conditions as you pointed out. We would like to encourage such experimental evaluations to be made on other spheres with different reflectances and designs.

To G. McKee

We have such a case in the realization of the lumen at NIST using an external source, where a beam flux is introduced through a sphere opening and incident on a small part of the sphere wall. In this case, we obtained a correction factor from that part of the SRDF (measured from the center of the sphere) and then applied a correction factor for the angle of incidence (in our case, the light hit at 45°). For a light source mounted at the sphere wall, the SRDF data (as obtained by simulation or measured by a scanning beam source at center of the sphere) can be converted to a hemispherical SRDF from that point of the sphere wall by applying corrections for angle of incidence. Such reflectance data (directional / hemispherical reflectance as a function of angle of incidence) of common diffuse materials are available in the past publications, or can be actually measured in the sphere.